EUROPEAN ORGANIZATION FOR NUCLEAR RESEARCH

CERN–EP/99–16

10 February 1999

# Measurement of the Lifetime of b-baryons

DELPHI Collaboration

**Abstract**

The average lifetime of weakly decaying $b$-baryons was studied using 3.6 million $Z^0$ hadronic decays collected by the DELPHI detector at LEP. The measurement of the proper decay time distribution of secondary vertices was used on three complementary samples. The first sample consisted of events with a fully reconstructed $\Lambda_c^+$ and an opposite charge lepton, or an oppositely charged lepton pair accompanied by a $\Lambda^0$. The other two samples were more inclusive, where $b$-baryon semileptonic decays were recognized by the presence of either a proton identified by the RICH detector or a $\Lambda^0$ and a lepton of charge opposite to that of the proton. The combined result was:

$$\tau(b-\text{baryon}) = 1.14 \pm 0.08\ (stat) \pm 0.04\ (syst)\ \text{ps}\ .$$

It updates and replaces all previous results published by the DELPHI collaboration.

(Submitted to Eur. Phys. J. C)

P.Abreu[21], W.Adam[50], T.Adye[36], P.Adzic[11], Z.Albrecht[17], T.Alderweireld[2], G.D.Alekseev[16], R.Alemany[49], T.Allmendinger[17], P.P.Allport[22], S.Almehed[24], U.Amaldi[9], S.Amato[47], E.G.Anassontzis[3], P.Andersson[44], A.Andreazza[9], S.Andringa[21], P.Antilogus[25], W-D.Apel[17], Y.Arnoud[9], B.Åsman[44], J-E.Augustin[25], A.Augustinus[9], P.Baillon[9], P.Bambade[19], F.Barao[21], G.Barbiellini[46], R.Barbier[25], D.Y.Bardin[16], G.Barker[17], A.Baroncelli[38], M.Battaglia[15], M.Baubillier[23], K-H.Becks[52], M.Begalli[6], P.Beilliere[8], Yu.Belokopytov[9,53], K.Belous[42], A.C.Benvenuti[5], C.Berat[14], M.Berggren[25], D.Bertini[25], D.Bertrand[2], M.Besancon[39], F.Bianchi[45], M.Bigi[45], M.S.Bilenky[16], M-A.Bizouard[19], D.Bloch[10], H.M.Blom[30], M.Bonesini[27], W.Bonivento[27], M.Boonekamp[39], P.S.L.Booth[22], A.W.Borgland[4], G.Borisov[19], C.Bosio[41], O.Botner[48], E.Boudinov[30], B.Bouquet[19], C.Bourdarios[19], T.J.V.Bowcock[22], I.Boyko[16], I.Bozovic[11], M.Bozzo[13], P.Branchini[38], T.Brenke[52], R.A.Brenner[48], P.Bruckman[18], J-M.Brunet[8], L.Bugge[32], T.Buran[32], T.Burgsmueller[52], P.Buschmann[52], S.Cabrera[49], M.Caccia[27], M.Calvi[27], T.Camporesi[9], V.Canale[37], F.Carena[9], L.Carroll[22], C.Caso[13], M.V.Castillo Gimenez[49], A.Cattai[9], F.R.Cavallo[5], V.Chabaud[9], M.Chapkin[42], Ph.Charpentier[9], L.Chaussard[25], P.Checchia[35], G.A.Chelkov[16], R.Chierici[45], P.Chliapnikov[42], P.Chochula[7], V.Chorowicz[25], J.Chudoba[29], K.Cieslik[18], P.Collins[9], R.Contri[13], E.Cortina[49], G.Cosme[19], F.Cossutti[9], J-H.Cowell[22], H.B.Crawley[1], D.Crennell[36], S.Crepe[14], G.Crosetti[13], J.Cuevas Maestro[33], S.Czellar[15], M.Davenport[9], W.Da Silva[23], A.Deghorain[2], G.Della Ricca[46], P.Delpierre[26], N.Demaria[9], A.De Angelis[9], W.De Boer[17], S.De Brabandere[2], C.De Clercq[2], B.De Lotto[46], A.De Min[35], L.De Paula[47], H.Dijkstra[9], L.Di Ciaccio[37,9], J.Dolbeau[8], K.Doroba[51], M.Dracos[10], J.Drees[52], M.Dris[31], A.Duperrin[25], J-D.Durand[9], G.Eigen[4], T.Ekelof[48], G.Ekspong[44], M.Ellert[48], M.Elsing[9], J-P.Engel[10], B.Erzen[43], M.Espirito Santo[21], E.Falk[24], G.Fanourakis[11], D.Fassouliotis[11], J.Fayot[23], M.Feindt[17], A.Fenyuk[42], P.Ferrari[27], A.Ferrer[49], E.Ferrer-Ribas[19], S.Fichet[23], A.Firestone[1], U.Flagmeyer[52], H.Foeth[9], E.Fokitis[31], F.Fontanelli[13], B.Franek[36], A.G.Frodesen[4], R.Fruhwirth[50], F.Fulda-Quenzer[19], J.Fuster[49], A.Galloni[22], D.Gamba[45], S.Gamblin[19], M.Gandelman[47], C.Garcia[49], C.Gaspar[9], M.Gaspar[47], U.Gasparini[35], Ph.Gavillet[9], E.N.Gazis[31], D.Gele[10], N.Ghodbane[25], I.Gil[49], F.Glege[52], R.Gokieli[9,51], B.Golob[43], G.Gomez-Ceballos[40], P.Goncalves[21], I.Gonzalez Caballero[40], G.Gopal[36], L.Gorn[1,54], M.Gorski[51], Yu.Gouz[42], V.Gracco[13], J.Grahl[1], E.Graziani[38], C.Green[22], H-J.Grimm[17], P.Gris[39], G.Grosdidier[19], K.Grzelak[51], M.Gunther[48], J.Guy[36], F.Hahn[9], S.Hahn[52], S.Haider[9], A.Hallgren[48], K.Hamacher[52], J.Hansen[32], F.J.Harris[34], V.Hedberg[24], S.Heising[17], J.J.Hernandez[49], P.Herquet[2], H.Herr[9], T.L.Hessing[34], J.-M.Heuser[52], E.Higon[49], S-O.Holmgren[44], P.J.Holt[34], S.Hoorelbeke[2], M.Houlden[22], J.Hrubec[50], K.Huet[2], G.J.Hughes[22], K.Hultqvist[44], J.N.Jackson[22], R.Jacobsson[9], P.Jalocha[9], R.Janik[7], Ch.Jarlskog[24], G.Jarlskog[24], P.Jarry[39], B.Jean-Marie[19], E.K.Johansson[44], P.Jonsson[25], C.Joram[9], P.Juillot[10], F.Kapusta[23], K.Karafasoulis[11], S.Katsanevas[25], E.C.Katsoufis[31], R.Keranen[17], B.P.Kersevan[43], B.A.Khomenko[16], N.N.Khovanski[16], A.Kiiskinen[15], B.King[22], A.Kinvig[22], N.J.Kjaer[30], O.Klapp[52], H.Klein[9], P.Kluit[30], P.Kokkinias[11], M.Koratzinos[9], V.Kostioukhine[42], C.Kourkoumelis[3], O.Kouznetsov[39], M.Krammer[50], E.Kriznic[43], J.Krstic[11], Z.Krumstein[16], P.Kubinec[7], J.Kurowska[51], K.Kurvinen[15], J.W.Lamsa[1], D.W.Lane[1], P.Langefeld[52], V.Lapin[42], J-P.Laugier[39], R.Lauhakangas[15], G.Leder[50], F.Ledroit[14], V.Lefebure[2], L.Leinonen[44], A.Leisos[11], R.Leitner[29], J.Lemonne[2], G.Lenzen[52], V.Lepeltier[19], T.Lesiak[18], M.Lethuillier[39], J.Libby[34], D.Liko[9], A.Lipniacka[44], I.Lippi[35], B.Loerstad[24], J.G.Loken[34], J.H.Lopes[47], J.M.Lopez[40], R.Lopez-Fernandez[14], D.Loukas[11], P.Lutz[39], L.Lyons[34], J.MacNaughton[50], J.R.Mahon[6], A.Maio[21], A.Malek[52], T.G.M.Malmgren[44], V.Malychev[16], J.Marco[40], R.Marco[40], B.Marechal[47], M.Margoni[35], J-C.Marin[9], C.Mariotti[9], A.Markou[11], C.Martinez-Rivero[19], F.Martinez-Vidal[49], S.Marti i Garcia[9], J.Masik[12], N.Mastroyiannopoulos[11], F.Matorras[40], C.Matteuzzi[27], G.Matthiae[37], F.Mazzucato[35], M.Mazzucato[35], M.Mc Cubbin[22], R.Mc Kay[1], R.Mc Nulty[22], G.Mc Pherson[22], C.Meroni[27], W.T.Meyer[1], E.Migliore[45], L.Mirabito[25], W.A.Mitaroff[50], U.Mjoernmark[24], T.Moa[44], M.Moch[17], R.Moeller[28], K.Moenig[9], M.R.Monge[13], X.Moreau[23], P.Morettini[13], G.Morton[34], U.Mueller[52], K.Muenich[52], M.Mulders[30], C.Mulet-Marquis[14], R.Muresan[24], W.J.Murray[36], B.Muryn[14,18], G.Myatt[34], T.Myklebust[32], F.Naraghi[14], F.L.Navarria[5], S.Navas[49], K.Nawrocki[51], P.Negri[27], S.Nemecek[12], N.Neufeld[9], N.Neumeister[50], R.Nicolaidou[39], B.S.Nielsen[28], M.Nikolenko[10,16], V.Nomokonov[15], A.Normand[22], A.Nygren[24], V.Obraztsov[42], A.G.Olshevski[16], A.Onofre[21], R.Orava[15], G.Orazi[10], K.Osterberg[15], A.Ouraou[39], M.Paganoni[27], S.Paiano[5], R.Pain[23], R.Paiva[21], J.Palacios[34], H.Palka[18], Th.D.Papadopoulou[31], K.Papageorgiou[11], L.Pape[9], C.Parkes[9], F.Parodi[13], U.Parzefall[22], A.Passeri[38], O.Passon[52], M.Pegoraro[35], L.Peralta[21], M.Pernicka[50], A.Perrotta[5], C.Petridou[46], A.Petrolini[13], H.T.Phillips[36], F.Pierre[39], M.Pimenta[21], E.Piotto[27], T.Podobnik[43], M.E.Pol[6], G.Polok[18], P.Poropat[46], V.Pozdniakov[16], P.Privitera[37], N.Pukhaeva[16], A.Pullia[27], D.Radojicic[34], S.Ragazzi[27], H.Rahmani[31], D.Rakoczy[50], P.N.Ratoff[20], A.L.Read[32], P.Rebecchi[9], N.G.Redaelli[27], M.Regler[50], D.Reid[30], R.Reinhardt[52], P.B.Renton[34], L.K.Resvanis[3], F.Richard[19], J.Ridky[12], G.Rinaudo[45], O.Rohne[32], A.Romero[45], P.Ronchese[35], E.I.Rosenberg[1], P.Rosinsky[7], P.Roudeau[19], T.Rovelli[5], Ch.Royon[39], V.Ruhlmann-Kleider[39], A.Ruiz[40], H.Saarikko[15], Y.Sacquin[39], A.Sadovsky[16], G.Sajot[14], J.Salt[49], D.Sampsonidis[11], M.Sannino[13], H.Schneider[17], Ph.Schwemling[23], U.Schwickerath[17], M.A.E.Schyns[52], F.Scuri[46], P.Seager[20], Y.Sedykh[16], A.M.Segar[34], R.Sekulin[36], R.C.Shellard[6], A.Sheridan[22], M.Siebel[52], L.Simard[39], F.Simonetto[35], A.N.Sisakian[16], G.Smadja[25], N.Smirnov[42], O.Smirnova[24], G.R.Smith[36], A.Sopczak[17], R.Sosnowski[51], T.Spassov[21], E.Spiriti[38], P.Sponholz[52], S.Squarcia[13], D.Stampfer[50], C.Stanescu[38], S.Stanic[43], K.Stevenson[34], A.Stocchi[19], J.Strauss[50], R.Strub[10], B.Stugu[4], M.Szczekowski[51], M.Szeptycka[51], T.Tabarelli[27], F.Tegenfeldt[48], F.Terranova[27], J.Thomas[34], J.Timmermans[30], N.Tinti[5], L.G.Tkatchev[16], S.Todorova[10], A.Tomaradze[2], B.Tome[21], A.Tonazzo[9], L.Tortora[38], G.Transtromer[24], D.Treille[9], G.Tristram[8], M.Trochimczuk[51], C.Troncon[27],

A.Tsirou[9], M-L.Turluer[39], I.A.Tyapkin[16], S.Tzamarias[11], B.Ueberschaer[52], O.Ullaland[9], V.Uvarov[42], G.Valenti[5], E.Vallazza[46], C.Vander Velde[2], G.W.Van Apeldoorn[30], P.Van Dam[30], W.K.Van Doninck[2], J.Van Eldik[30], A.Van Lysebetten[2], I.Van Vulpen[30], N.Vassilopoulos[34], G.Vegni[27], L.Ventura[35], W.Venus[36,9], F.Verbeure[2], M.Verlato[35], L.S.Vertogradov[16], V.Verzi[37], D.Vilanova[39], L.Vitale[46], E.Vlasov[42], A.S.Vodopyanov[16], C.Vollmer[17], G.Voulgaris[3], V.Vrba[12], H.Wahlen[52], C.Walck[44], C.Weiser[17], D.Wicke[52], J.H.Wickens[2], G.R.Wilkinson[9], M.Winter[10], M.Witek[18], G.Wolf[9], J.Yi[1], O.Yushchenko[42], A.Zaitsev[42], A.Zalewska[18], P.Zalewski[51], D.Zavrtanik[43], E.Zevgolatakos[11], N.I.Zimin[16,24], G.C.Zucchelli[44], G.Zumerle[35]

[1] Department of Physics and Astronomy, Iowa State University, Ames IA 50011-3160, USA
[2] Physics Department, Univ. Instelling Antwerpen, Universiteitsplein 1, BE-2610 Wilrijk, Belgium
and IIHE, ULB-VUB, Pleinlaan 2, BE-1050 Brussels, Belgium
and Faculté des Sciences, Univ. de l'Etat Mons, Av. Maistriau 19, BE-7000 Mons, Belgium
[3] Physics Laboratory, University of Athens, Solonos Str. 104, GR-10680 Athens, Greece
[4] Department of Physics, University of Bergen, Allégaten 55, NO-5007 Bergen, Norway
[5] Dipartimento di Fisica, Università di Bologna and INFN, Via Irnerio 46, IT-40126 Bologna, Italy
[6] Centro Brasileiro de Pesquisas Físicas, rua Xavier Sigaud 150, BR-22290 Rio de Janeiro, Brazil
and Depto. de Física, Pont. Univ. Católica, C.P. 38071 BR-22453 Rio de Janeiro, Brazil
and Inst. de Física, Univ. Estadual do Rio de Janeiro, rua São Francisco Xavier 524, Rio de Janeiro, Brazil
[7] Comenius University, Faculty of Mathematics and Physics, Mlynska Dolina, SK-84215 Bratislava, Slovakia
[8] Collège de France, Lab. de Physique Corpusculaire, IN2P3-CNRS, FR-75231 Paris Cedex 05, France
[9] CERN, CH-1211 Geneva 23, Switzerland
[10] Institut de Recherches Subatomiques, IN2P3 - CNRS/ULP - BP20, FR-67037 Strasbourg Cedex, France
[11] Institute of Nuclear Physics, N.C.S.R. Demokritos, P.O. Box 60228, GR-15310 Athens, Greece
[12] FZU, Inst. of Phys. of the C.A.S. High Energy Physics Division, Na Slovance 2, CZ-180 40, Praha 8, Czech Republic
[13] Dipartimento di Fisica, Università di Genova and INFN, Via Dodecaneso 33, IT-16146 Genova, Italy
[14] Institut des Sciences Nucléaires, IN2P3-CNRS, Université de Grenoble 1, FR-38026 Grenoble Cedex, France
[15] Helsinki Institute of Physics, HIP, P.O. Box 9, FI-00014 Helsinki, Finland
[16] Joint Institute for Nuclear Research, Dubna, Head Post Office, P.O. Box 79, RU-101 000 Moscow, Russian Federation
[17] Institut für Experimentelle Kernphysik, Universität Karlsruhe, Postfach 6980, DE-76128 Karlsruhe, Germany
[18] Institute of Nuclear Physics and University of Mining and Metalurgy, Ul. Kawiory 26a, PL-30055 Krakow, Poland
[19] Université de Paris-Sud, Lab. de l'Accélérateur Linéaire, IN2P3-CNRS, Bât. 200, FR-91405 Orsay Cedex, France
[20] School of Physics and Chemistry, University of Lancaster, Lancaster LA1 4YB, UK
[21] LIP, IST, FCUL - Av. Elias Garcia, 14-1$^{o}$, PT-1000 Lisboa Codex, Portugal
[22] Department of Physics, University of Liverpool, P.O. Box 147, Liverpool L69 3BX, UK
[23] LPNHE, IN2P3-CNRS, Univ. Paris VI et VII, Tour 33 (RdC), 4 place Jussieu, FR-75252 Paris Cedex 05, France
[24] Department of Physics, University of Lund, Sölvegatan 14, SE-223 63 Lund, Sweden
[25] Université Claude Bernard de Lyon, IPNL, IN2P3-CNRS, FR-69622 Villeurbanne Cedex, France
[26] Univ. d'Aix - Marseille II - CPP, IN2P3-CNRS, FR-13288 Marseille Cedex 09, France
[27] Dipartimento di Fisica, Università di Milano and INFN, Via Celoria 16, IT-20133 Milan, Italy
[28] Niels Bohr Institute, Blegdamsvej 17, DK-2100 Copenhagen Ø, Denmark
[29] NC, Nuclear Centre of MFF, Charles University, Areal MFF, V Holesovickach 2, CZ-180 00, Praha 8, Czech Republic
[30] NIKHEF, Postbus 41882, NL-1009 DB Amsterdam, The Netherlands
[31] National Technical University, Physics Department, Zografou Campus, GR-15773 Athens, Greece
[32] Physics Department, University of Oslo, Blindern, NO-1000 Oslo 3, Norway
[33] Dpto. Fisica, Univ. Oviedo, Avda. Calvo Sotelo s/n, ES-33007 Oviedo, Spain
[34] Department of Physics, University of Oxford, Keble Road, Oxford OX1 3RH, UK
[35] Dipartimento di Fisica, Università di Padova and INFN, Via Marzolo 8, IT-35131 Padua, Italy
[36] Rutherford Appleton Laboratory, Chilton, Didcot OX11 OQX, UK
[37] Dipartimento di Fisica, Università di Roma II and INFN, Tor Vergata, IT-00173 Rome, Italy
[38] Dipartimento di Fisica, Università di Roma III and INFN, Via della Vasca Navale 84, IT-00146 Rome, Italy
[39] DAPNIA/Service de Physique des Particules, CEA-Saclay, FR-91191 Gif-sur-Yvette Cedex, France
[40] Instituto de Fisica de Cantabria (CSIC-UC), Avda. los Castros s/n, ES-39006 Santander, Spain
[41] Dipartimento di Fisica, Università degli Studi di Roma La Sapienza, Piazzale Aldo Moro 2, IT-00185 Rome, Italy
[42] Inst. for High Energy Physics, Serpukov P.O. Box 35, Protvino, (Moscow Region), Russian Federation
[43] J. Stefan Institute, Jamova 39, SI-1000 Ljubljana, Slovenia and Laboratory for Astroparticle Physics,
Nova Gorica Polytechnic, Kostanjeviska 16a, SI-5000 Nova Gorica, Slovenia,
and Department of Physics, University of Ljubljana, SI-1000 Ljubljana, Slovenia
[44] Fysikum, Stockholm University, Box 6730, SE-113 85 Stockholm, Sweden
[45] Dipartimento di Fisica Sperimentale, Università di Torino and INFN, Via P. Giuria 1, IT-10125 Turin, Italy
[46] Dipartimento di Fisica, Università di Trieste and INFN, Via A. Valerio 2, IT-34127 Trieste, Italy
and Istituto di Fisica, Università di Udine, IT-33100 Udine, Italy
[47] Univ. Federal do Rio de Janeiro, C.P. 68528 Cidade Univ., Ilha do Fundão BR-21945-970 Rio de Janeiro, Brazil
[48] Department of Radiation Sciences, University of Uppsala, P.O. Box 535, SE-751 21 Uppsala, Sweden
[49] IFIC, Valencia-CSIC, and D.F.A.M.N., U. de Valencia, Avda. Dr. Moliner 50, ES-46100 Burjassot (Valencia), Spain
[50] Institut für Hochenergiephysik, Österr. Akad. d. Wissensch., Nikolsdorfergasse 18, AT-1050 Vienna, Austria
[51] Inst. Nuclear Studies and University of Warsaw, Ul. Hoza 69, PL-00681 Warsaw, Poland
[52] Fachbereich Physik, University of Wuppertal, Postfach 100 127, DE-42097 Wuppertal, Germany
[53] On leave of absence from IHEP Serpukhov
[54] Now at University of Florida

# 1 Introduction

The weak decays of baryons containing a beauty quark, referred to as $b$-baryons throughout this paper, were observed in $Z^0$ hadronic decays at LEP [1,2] by the correlation found between $\Lambda^0$or $\Lambda_c^+$particles and leptons. Using this correlation, first measurements of the average $b$-baryon lifetime were made [2,3]. Theoretical predictions give for this quantity values only 5% to 10% less than the B meson lifetime [4]. However, current experimental results [5–7] indicate a substantially shorter lifetime which is difficult to accommodate theoretically. This paper updates the previous DELPHI publications and benefits from the final data set and detector calibration.

The $b$-baryon lifetime was measured using the proper time distribution of decays at secondary vertices. The first sample used partially reconstructed $b$-baryon decay candidates, containing a $\Lambda_c^+$ correlated with a high momentum lepton, or a $\Lambda^0$ correlated with a pair of oppositely charged leptons, originating from the semileptonic decay of a $b$-baryon into a charmed baryon, followed by the semileptonic decay of the charmed baryon into $\Lambda^0 \ell^+ \nu_\ell X$.

Two more inclusive analyses are also reported, where the presence of the beauty quark was tagged by a high momentum lepton; $b$-baryon decay candidates were selected by the presence of a proton or a $\Lambda^0$ among the particles coming from the secondary vertex, taking advantage of the proton identification capability of the DELPHI detector.

The signal events selected in these analyses are a mixture of different $b$-baryon types, weighted by their production rates at LEP and selection efficiencies. But, as it will be shown below, the average lifetime measured, referred to as $b$-baryon lifetime, was essentially sensitive to that of $\Lambda_b^0$'s.

As the branching fractions of the decays involved are poorly known, it was important to measure the sample compositions and background lifetimes in the data. In the following, the inclusion of charge conjugate states will always be implied.

# 2 Event reconstruction with the DELPHI Detector

The DELPHI detector and its performance have been described in detail elsewhere [8,9]. In this section are summarised the most relevant characteristics for this analysis.

## 2.1 Global event reconstruction

### 2.1.1 Charged particle reconstruction

The detector elements used for tracking were the Vertex Detector (VD), the Inner Detector (ID), the Time Projection Chamber (TPC) and the Outer Detector (OD).

The VD provided the high precision needed near the primary vertex. For the data taken from 1991 to 1993, the VD consisted of three cylindrical layers of silicon detectors (radii 6.3, 9.0 and 10.9 cm) measuring points in the plane transverse to the beam direction ($r\phi$ coordinate) in the polar angle range $43^\circ < \theta < 137^\circ$. In 1994, two layers were equipped with detector modules with double sided readout, providing a single hit precision of 7.6 $\mu$m in the $r\phi$ coordinate, similar to that obtained previously, and 9 $\mu$m in the coordinate parallel to the beam ($z$) [10]. For high momentum particles with associated hits in the VD, the extrapolation precision close to the interaction region was 20 $\mu$m in the $r\phi$ plane and 34 $\mu$m in the $rz$ plane.

Charged particle tracks were reconstructed with 95% efficiency and with a momentum resolution $\sigma_p/p < 2.0 \times 10^{-3} p$ ($p$ in GeV/$c$) in the polar angle region $25° < \theta < 155°$.

### 2.1.2 Energy reconstruction

The total energy in the event was determined by using all information available from the tracking detectors and the calorimeters. For charged particles, the momentum measured in the tracking detector was used. Photons were detected and their energy measured in the electromagnetic calorimeters, whereas the hadron calorimeter detected long lived neutral hadrons such as neutrons and $K^0_L$'s.

The electromagnetic calorimetry system of DELPHI was composed of a barrel calorimeter, the HPC, covering the polar angle region $46° < \theta < 134°$, and a forward calorimeter, the FEMC, for polar angles $8° < \theta < 35°$ and $145° < \theta < 172°$. The relative precision on the measured energy $E$ was parametrised as $\sigma_E/E = 0.32/\sqrt{E} \oplus 0.043$ ($E$ in GeV) in the barrel, and $\sigma_E/E = 0.12/\sqrt{E} \oplus 0.03$ ($E$ in GeV) in the forward region.

The hadron calorimeter, HCAL, was installed in the return yoke of the DELPHI solenoid. In the barrel region, the energy was reconstructed with a precision of $\sigma_E/E = 1.12/\sqrt{E} \oplus 0.21$ ($E$ in GeV).

### 2.1.3 Hadronic $Z^0$ selection

Hadronic events from $Z^0$ decays were selected by requiring a charged multiplicity greater than four and a total energy of charged particles greater than $0.12\sqrt{s}$, where $\sqrt{s}$ is the centre-of-mass energy and all particles were assumed to be pions; charged particles were required to have a momentum greater than 0.4 GeV/$c$ and a polar angle between 20° and 160°. The overall trigger and selection efficiency was (95.0±0.1)% [11]. A total of 3.6 million hadronic events was obtained from the 1992-1995 data.

## 2.2 Particle identification

### 2.2.1 Lepton identification

Lepton identification in the DELPHI detector was based on the barrel electromagnetic calorimeter and the muon chambers. Only particles with momentum larger than 2 GeV/$c$ were considered as possible lepton candidates.

Two layers of muon chambers covered the polar angle region $20° < \theta < 160°$, except for two regions of ±3° around $\theta = 42°$ and $\theta = 138°$. The first layer consisted of three planes of chambers and was inside the return yoke of the magnet after 90 cm of iron, while the second, with two chamber planes, was mounted outside the yoke behind a further 20 cm of iron. The probability of a particle being a muon was calculated from a global $\chi^2$ of the match between the track extrapolation to the muon chambers and the hits observed there. With the selections applied, the muon identification efficiency was $(86 \pm 1)\%$ and the hadron misidentification probability $(0.7 \pm 0.1)\%$.

The probability of a particle being an electron was calculated using a) the spatial separation between its extrapolated position at the HPC and the position of the nearest electromagnetic shower, b) a comparison between its momentum and the measured energy, and c) a successful fit to the longitudinal profile of the shower in the nine HPC layers. The measurement of the $dE/dx$ in the TPC (described in section 2.2.2), was used in the algorithm as independent and complementary information. With the selections ap-

plied and inside the angular acceptance of the HPC, the electron identification efficiency was found to be $(65 \pm 1)\%$ and the hadron misidentification probability 0.4%.

### 2.2.2 Hadron identification

Hadron identification relied on the RICH detector and on the specific ionisation measurement performed by the TPC.

The RICH detector [12] used two radiators. A gas radiator separated protons from pions between 3 and 15 GeV/$c$, where protons gave no Cherenkov light whereas pions did, and between 15 and 20 GeV/$c$, using the measured Cherenkov angle. It also provided proton/kaon separation from 8 to 20 GeV/$c$. A liquid radiator, which was fully operational for 1994 and 1995 data, provided $p/K/\pi$ separation in the momentum range 1.5–7 GeV/$c$.

The combination of the information of the two radiators provided proton identification up to 20 GeV/$c$, with a constant efficiency of 70%. The proton/pion rejection factor, defined as the ratio between the percentage of protons correctly identified and the percentage of pions misidentified as protons, was about 10. A similar rejection factor was obtained for the proton/kaon separation between 1.5 and 6 GeV/$c$ using the liquid radiator, and between 8 and 20 GeV/$c$ using the gas radiator. Between 6 and 8 GeV/$c$, proton/kaon separation was obtained with a poorer efficiency. As a consequence, for the analyses where both pion and kaon rejections were needed, the efficiency depended on the particle momentum: for the analyses presented here, the efficiency, averaged on the full momentum spectrum, was 35%.

The specific energy loss ($dE/dx$) was measured in the TPC by using up to 192 sense wires. At least 30 contributing measurements were required to compute the truncated mean. In the momentum range $3 < p < 25$ GeV/$c$, this was fulfilled for 55% of the tracks, and the $dE/dx$ measurement had a precision of $\pm 7\%$.

For the semi-exclusive channels, which used invariant mass cuts to select the $b$-baryon events, or for decays involving a $\Lambda^0$, only a loose proton identification was required, and the RICH and $dE/dx$ information were combined, using the "or" of the two flags.

In the proton-lepton analysis, for which the B meson rejection relied only on particle identification, only 1994 and 1995 data were used. In a first step, only the RICH was used to identify protons. The $dE/dx$ information was used to measure the resulting purity and to estimate the corresponding systematic uncertainty. Then, particles for which the measured $dE/dx$ was incompatible with the expectation for a proton were rejected.

### 2.2.3 $\Lambda^0$ and $K^0$ reconstruction

The $\Lambda^0 \to p\pi^-$ and $K^0 \to \pi^+\pi^-$ decays were reconstructed if the distance in the $r\phi$ plane between the $\Lambda^0$ decay point and the primary vertex was less than 90 cm. This condition meant that the decay products had track segments at least 20 cm long in the TPC. The reconstruction of the $V^0$ vertex and selection cuts are described in detail in reference [9].

For $K^0$'s, the $\pi^+\pi^-$ invariant mass was required to lie between 0.475 and 0.525 GeV/$c^2$. For $\Lambda^0$'s, the particle with the highest momentum was assumed to be the proton, and the $p\pi$ invariant mass was required to lie between 1.08 and 1.18 GeV/$c^2$. In addition, the $\Lambda^0$ candidate was rejected if the $dE/dx$ or the Cherenkov angle measured for the proton candidate were incompatible with the values expected for a proton. It was also required that neither the proton nor the pion were identified as a lepton. This reduced the combinatorial background by about a factor of two, with negligible efficiency loss.

For the considered decay modes, the $\Lambda^0/K^0$ momentum varied between 2 GeV/$c$ and 20 GeV/$c$. The $K^0 \to \pi^+\pi^-$ and $\Lambda^0 \to p\pi^-$ reconstruction efficiencies depended strongly on the $V^0$ momentum, and varied between 35% and 10%.

## 2.3 Primary and secondary vertex reconstruction

The primary vertex of the $e^+e^-$ interaction was reconstructed on an event-by-event basis using the beam spot position as a constraint [9]. In 1994 and 1995 data, the position of the primary vertex, transverse to the beam, was determined with a precision of about 40 $\mu$m in the horizontal direction, and about 10 $\mu$m in the vertical direction. For 1992 and 1993 data, the uncertainties were larger by about 50%.

The event was divided into two hemispheres, using the plane perpendicular to the event thrust axis. The particles were clustered into jets (using the LUCLUS algorithm [13]), and the search for a secondary vertex was triggered in the jets where a high momentum lepton was identified. The track selection and secondary vertex reconstruction were different for the exclusive and inclusive analyses, and will be described in detail in the corresponding sections. Due to the precision of the track extrapolation obtained with the VD, secondary vertices from beauty and charm hadron decays were reconstructed with a precision of about 300 $\mu$m along the flight direction of the decaying particle.

The sum of the momenta of the particles attached to the secondary vertex was used to estimate the energy of the incoming particle, $E_{b-baryon}$. The "residual energy" method, described in more detail in [7,14,15], was used to evaluate the missing energy in the $b$-baryon decay. First, the energies of all particles attached to the secondary vertex were added, defining the quantity $E_{sec}$. The total energy $E_{vis}$ in the hemisphere containing the secondary vertex was computed. The $b$-baryon energy was then defined to be:

$$E_{b-baryon} = E_{beam} - E_{res} = E_{beam} - (E_{vis} - E_{sec}) \; . \qquad (1)$$

The resulting resolution on the $b$-baryon momentum was $\Delta p/p = 15\%$. Possible differences between data and the simulation prediction were studied using B meson semileptonic decays, which have similar properties to those of $b$-baryons and are better known. They were used to check that the detector behaviour was well described by the simulation, in particular concerning the estimation of the $b$-baryon momentum.

For each event, the decay time was computed from the formula: $t = M_{\Lambda_b^0} L/p$, where $M_{\Lambda_b^0}$ is the $\Lambda_b^0$ mass [16], $L$ the distance between the primary and secondary vertices and $p$ the $b$-baryon momentum. A typical resolution of 0.20 ps was obtained.

## 2.4 $b$-tagging

Charged particle tracks from the hemisphere opposite to that of the reconstructed vertex were used to enrich the samples in events containing $b$-hadrons, without distorting the distribution of the secondary vertex flight distance. The $b$-tagging package developed by the DELPHI collaboration has been described in reference [17]. The impact parameters of the charged particle tracks, with respect to the primary vertex, were used to build the probability that all tracks come from the primary vertex. Due to the long $b$-hadron lifetime, the probability distribution was peaked at zero for events which contained beauty whereas it was flat for events containing light quarks. Demanding a probability smaller than 0.1 rejected 70% of the events which contained no beauty quark. The distributions of the $b$-tagging probability were compared in data and simulation, and agreed within 3% . The residual correlation between the two hemispheres, due to the common primary

vertex, was also studied, and found to be negligible compared to the precision expected on the lifetime measurement.

# 3 Event simulation

The DELPHI simulation program [9] included a full simulation of the detector response. It used the PYTHIA event generator and the JETSET Parton Shower program for the quark fragmentation [13]. About 5 million simulated $Z^0$ hadronic decays were used in the analysis.

The simulation was tuned to match the experimentally observed $b$-baryon production rate and decay properties. Events were reweighted to accomodate the most recent measurements and to estimate the systematic uncertainty related to the model assumptions.

- $b$-baryon production:
  The uncertainty on the total $b$-baryon production fraction from $b$ jets at LEP is large [6], but did not affect the analyses presented here because the sample compositions have been measured on data. Various types of $b$-baryons produced in $Z^0$ decays, $\Lambda_b^0$'s but also $\Xi_b$'s, which might have different lifetimes. The fraction of $\Xi_b$'s among the $b$-baryons produced at LEP is presently known with a precision of $\pm 30\%$ [16,18], and has been set to 14% in the simulation. However, after secondary vertex reconstruction and selection criteria, the $\Xi_b$ contribution to the signal was found to be negligible in the $\Lambda_c^+\ell$ sample, and only of about 2% in the proton-lepton channel. Other $b$-baryons, like $\Sigma_b$'s or $\Sigma_b^*$'s, decay immediately into $\Lambda_b^0$ by strong interaction. Therefore, the average lifetime measured is essentially that of the $\Lambda_b^0$.
- $b$-baryon momentum spectrum and semileptonic decay:
  The fragmentation function of the $b$-quark into $b$-baryons has never been measured. But the mass difference between B mesons and $b$-baryons is such that their fragmentation functions are expected to be almost identical. Therefore, the average value of the $b$-baryon energy was assumed to be the same as the average value measured for $b$ hadrons ($\langle E_{b-hadron}/E_{beam}\rangle = 0.715 \pm 0.030$ [19]), and possible difference between the $b$ quark fragmentation distributions into mesons and baryons were included in the systematic uncertainties. The $b$-baryon semileptonic decays were simulated in the framework of the Heavy Quark Effective Theory, using the Isgur-Wise function [20]. The generated lifetime of all B mesons and $b$-baryons was set to 1.6 ps in the DELPHI simulation, and events were reweighted to mimic shorter $b$-baryon lifetimes.
- $\Lambda_b^0$ mass and decay modes:
  The $\Lambda_b^0$ baryon mass entered in the decay time calculation but, due to a recent accurate measurement ($5624 \pm 9$ GeV/$c^2$ [16,21]), the related uncertainty was negligible. The simulation predicted that 90% of the $\Lambda_b^0$ semileptonic decays proceeded via a $\Lambda_c^+$. Non-resonant $\Lambda_b^0 \to \Lambda_c^+(\mathrm{n}\pi)\ell^-\bar{\nu}_\ell$ decays (where n is a positive integer) might be an important fraction of the total decay width. The effect on the $b$-baryon momentum estimation was studied in detail, using special simulated samples. The $\Lambda_b^0$ polarisation modifies the distribution of the impact parameter of the lepton (with respect to the primary vertex) but did not affect the analyses presented here, where the $\Lambda_b^0$ decay vertex was reconstructed.
- $\Lambda_c^+$ decay:
  In both semi-exclusive and inclusive analyses, the selected signal events occurred through several $\Lambda_c^+$ decay channels for which the precision on the secondary vertex

reconstruction could be different. For example, the proton-lepton sample contained $\Lambda_c^+ \to \Lambda^0 X$ decays, where the $\Lambda^0$ was not reconstructed and for which the secondary vertex reconstruction was slightly deteriorated compared to direct $\Lambda_c^+ \to pX$ decays (without $\Lambda^0$). Similarly, the $b$-baryon momentum reconstruction could be affected when the $\Lambda_c^+$ decay involved some $\pi^0$ or $K_L^0$, which might escape detection. The presently measured $\Lambda_c^+$ decay branching ratios [16,22] have large uncertainties. Simulated events were reweighted accordingly: as discussed below, all effects were found to be very small.

# 4 Lifetime measurement using $\Lambda_c^+\ell^-$ and $\Lambda^0\ell^-\ell^+$ samples

The analysis presented in this section used $\Lambda_b^0 \to \Lambda_c^+\ell^-\bar{\nu}_\ell$ decays, with the $\Lambda_c^+$ either fully reconstructed in a hadronic decay mode or partially reconstructed in the semileptonic decay $\Lambda_c^+ \to \Lambda^0\ell^+\nu_\ell X$. The decay time distribution obtained from the observed distance between the reconstructed vertices and from the estimated $\Lambda_b^0$ momentum was fitted, using the likelihood function described below, to determine the average $b$-baryon lifetime.

## 4.1 Selection of the $\Lambda_c^+\ell^-$ sample

Fully reconstructed $\Lambda_c^+ \to pK^-\pi^+$, $\Lambda_c^+ \to \bar{K^0}p$ and $\Lambda_c^+ \to p\bar{K^0}\pi^+\pi^-$ decays were correlated with the presence of a $\ell^-$ in the same hemisphere. This analysis extended the study presented in detail in [7] to the full data set. It also benefitted from the final detector calibration and data processing, and the combined identification from the RICH and TPC detectors. The $b$-tagging selection discussed in section 4.2 was used.

The $\Lambda_c^+$ candidates were paired with identified leptons of momentum above 3 GeV/$c$, within a cone of half angle 1.2 rad around the $\Lambda_c^+$ direction. The lepton transverse momentum with respect to the jet axis, $p_\ell^T$, was computed including the lepton itself inside the jet. The requirements on the properties of $\Lambda_c^+$ decay products and of the $\Lambda_c^+\ell^-$ pairs are reported in Table 1.

The mass plots for the $\Lambda_c^+$ candidates are shown in Figure 1 for the three considered channels. The $\Lambda_c^+$ candidate decay products had to fit a common vertex with a probability larger than 0.001. The line of flight had to be within a cone of half angle 10° relative to the reconstructed momentum direction. The $b$-baryon decay vertex was reconstructed using the trajectories of the $\Lambda_c^+$ and of the lepton fitted to a common vertex, except for the $\Lambda_c^+ \to p\bar{K^0}$ channel where the proton-lepton vertex was used.

147 vertices were selected in the right sign $\Lambda_c^+\ell^-$ combination and in the signal mass region (with $2.260 < M(\Lambda_c^+) < 2.330$ GeV/$c^2$), shown by the arrows in Figure 2a. 888 background vertices were selected in the wrong sign $\Lambda_c^+\ell^+$ combination (with $2.100 < M(\Lambda_c^+) < 2.400$ GeV/$c^2$ ) and in the right sign combination but outside the signal region (with $2.100 < M(\Lambda_c^+) < 2.220$ GeV/$c^2$ or $2.350 < M(\Lambda_c^+) < 2.400$ GeV/$c^2$).

The $b$-baryon momentum was estimated with the residual energy method described in section 2.3. The positions of the primary and decay vertices were used to measure the decay distance.

Table 1: Selection cuts on $\Lambda_c^+$ decay products and on $\Lambda_c^+$-lepton candidates. $p_i$ and $p_i^T$ are the momentum and transverse momentum of the particle $i$, $p_{(\Lambda_c^+\ell)}$ and $M(\Lambda_c^+\ell)$ are the total momentum and invariant mass of the $(\Lambda_c^+\ell)$ system.

| $\Lambda_c^+$ decay channel | Kinematical variable | Accepted range |
|---|---|---|
| $\Lambda_c^+ \to pK^-\pi^+$ | $p_p$ | $> 3.0$ GeV/$c$ |
| " | $p_K$ | $> 2.0$ GeV/$c$ |
| " | $p_\pi$ | $> 1.0$ GeV/$c$ |
| $\Lambda_c^+ \to p\bar{K}^0$ | $p_p$ | $> 3.0$ GeV/$c$ |
| " | $p_{K^0}$ | $> 2.0$ GeV/$c$ |
| $\Lambda_c^+ \to p\bar{K}^0\pi^+\pi^-$ | $p_p$ | $> 3.0$ GeV/$c$ |
| " | $p_{K^0}$ | $> 1.5$ GeV/$c$ |
| " | $p_\pi$ | $> 0.8$ GeV/$c$ |
| all | $p_{\Lambda_c^+}$ | $> 8.0$ GeV/$c$ |
| " | $p_\ell$ | $> 3.0$ GeV/$c$ |
| " | $p_\ell^T$ | $> 0.6$ GeV/$c$ |
| " | $p_{(\Lambda_c^+\ell)}$ | $> 16.0$ GeV/$c$ |
| " | $M(\Lambda_c^+\ell)$ | $3.4 < M < 5.5$ GeV/$c^2$ |

## 4.2 Selection of the $\Lambda^0\ell^-\ell^+$ sample

In the decay channel $\Lambda_b^0 \to \Lambda_c^+\ell^-\bar{\nu}_\ell X$ with $\Lambda_c^+ \to \Lambda^0\ell^+\nu_\ell X'$ and $\Lambda^0 \to p\pi^-$, where $X$ and $X'$ are any particles, the $\Lambda^0$ was combined with a pair of oppositely charged leptons. This decay channel was used to adjust the selection cuts, although this analysis is sensitive to $b$-baryon semileptonic decays into any $c$-baryon, followed by the semileptonic decay of the $c$-baryon into $\Lambda^0\ell^+\nu_\ell X$.

The lepton from the semileptonic decay of the $b$-baryon is expected to have a high transverse and a high longitudinal momentum with respect to the jet axis. The lepton candidate with the highest $p_{\rm T}$ was required to have a momentum greater than 3 GeV/$c$, a $p_{\rm T}$ value larger than 0.5 GeV/$c$ and a charge opposite to that of the proton from the $\Lambda^0$ decay. The second lepton was required to have a momentum greater than 2 GeV/$c$, a $p_{\rm T}$ value larger than 0.2 GeV/$c$ and the same charge as the proton. This combination will be referred to as "right sign" in the following. The "wrong sign" combination groups events in which the two leptons had same charge, and events in which the lepton with the highest $p_{\rm T}$ had the same charge as the proton.

The $b$-tagging selection discussed in section 2.4 was used. Due to the presence of two consecutive semileptonic decays, the average number of charged particles was reduced in such events. Therefore a further background reduction was obtained by requiring less than 10 particles within a cone of half angle 18° from both lepton directions. The $\Lambda^0$ reconstruction and selection was described in section 2.2.3. Since the $\Lambda^0$ from the $\Lambda_c^+$ decay typically had a harder momentum spectrum than that of $\Lambda^0$'s produced in light quark fragmentation, the momentum of the $\Lambda^0$ candidate in the selection of $\Lambda^0\ell^-\ell^+$ events was required to be greater than 4 GeV/$c$.

The $\Lambda_b^0$ momentum was estimated with the residual energy method mentioned in section 2.3. The resulting $p_{\Lambda_b^0}$ was required to be greater than 18 GeV/$c$. The invariant mass of the $\Lambda^0\ell^-\ell^+$ was required to be between 2.1 GeV/$c^2$ and 4.5 GeV/$c^2$ and $M(\Lambda^0\ell^+)$ had to be less than 2.3 GeV/$c^2$.

With these requirements 22 "right sign" events were selected in the "peak region" $1.104 < M(p\pi) < 1.132$ GeV/$c^2$, as shown in Figure 2b. The corresponding "wrong sign" peak in Figure 2e contained 9 events. This could be compared with the predictions obtained by studying a simulated sample of 5 million $Z^0$ hadronic decays, i.e. 1.4 times the data set, which gave 39 "right sign" events and 11 "wrong sign" events in the peak region. In the simulated sample, 25 "right sign" events were true $\Lambda_b \to \Lambda_c^+ \ell^- \bar{\nu}_\ell X$ decays with $\Lambda_c^+ \to \Lambda^0 \ell^+ \nu_\ell X'$. The rest of the sample mainly came from fake $\Lambda^0$'s, or $\Lambda_b$ decays with a true $\Lambda^0$ combined with a true lepton from the semileptonic $b$-decay, and a misidentified second lepton. The probability of interchanging the two leptons was also studied in the simulated events, but this contribution was found to be negligible.

For each event a vertex was fitted using the two lepton tracks, giving an estimate for the decay distance of the $\Lambda_b$. Since the second lepton came from the $\Lambda_c^+$ decay, this gave an overestimated decay distance. This distance had thus to be multiplied by a factor $0.90 \pm 0.03$, obtained by equalizing the average estimated distance with the generated one in the simulated sample. Using only the $\Lambda^0$ and the first lepton track was also investigated, but this was found to give a poor reconstruction of the $\Lambda_b$ decay vertex. Due to the residual energy method, the presence of the additional neutrino did not affect the $b$-baryon momentum estimation and no correction was needed.

## 4.3 Likelihood function for the lifetime fit

The lifetime fit was performed using the $\Lambda_c^+ \ell^-$ and $\Lambda^0 \ell^- \ell^+$ samples together. The signal and background lifetimes were determined by fitting the "right sign" and "wrong sign" samples simultaneously.

For each event $i$, the decay time $t_i$ was computed as explained in section 2.3. The uncertainty $\sigma_i$ on the measured decay time $t_i$ was computed from the quadratic sum of the relative errors on the secondary vertex position, computed for each event, and on the $b$-baryon momentum, estimated to be 15%. The likelihood function used in the lifetime fit was the sum of four contributions parametrising the signal and background behaviour:

$$\ln L = \Sigma_i \ln f(t_i, \sigma_i, \tau, f_1, f_2, \tau_1, \tau_2) \tag{2}$$

with

$$\begin{aligned} f(t_i, \sigma_i, \tau, f_1, f_2, \tau_1, \tau_2) = f_{signal} \cdot P(t_i, \tau, \sigma_i) \; + \\ (1 - f_{signal}) \cdot [f_1 \cdot P(t_i, \tau_1, \sigma_i) + f_2 \cdot P(t_i, \tau_2, \sigma_i) + (1 - f_1 - f_2) \cdot F(t_i, \sigma_i)] \; . \end{aligned} \tag{3}$$

The signal fraction, $f_{signal}$, was parametrised for each decay channel as a function of the reconstructed $\Lambda_c^+$ ($\Lambda^0$) invariant mass, using the distributions shown in Figures 1 and 2b,e. For the "right sign" combination its value, averaged over various channels, was $(56 \pm 6)\%$. For "wrong sign" events, the contribution of $b$-baryons was small and $f_{signal}$ was set to zero.

The function $P(t_i, \tau, \sigma_i)$ was the convolution of an exponential function with an average lifetime $\tau$ and a Gaussian resolution function of width $\sigma_i$. The reconstruction efficiency was found to be independent of the decay time and no acceptance correction was needed.

The background with null lifetime, due to vertices reconstructed in $u, d, s$ events, was parametrised, using the simulation, as the sum $F(t_i, \sigma_i)$ of Gaussian functions. The "flying background" had a lifetime shape very close to an exponential, with an "effective" lifetime $\tau_1$. But a better fit stability was obtained by adding a second contribution, of "effective" lifetime $\tau_2$. As for the signal, the function $P(t_i, \tau_j, \sigma_i)$ was the convolution

between the exponential function of lifetime $\tau_j$ and a Gaussian resolution function of width $\sigma_i$.

The fit had five free parameters: the signal lifetime $\tau$, and the four parameters $f_1, f_2, \tau_1, \tau_2$ describing the flying background composition and shape. The proper time distributions with the fit result are shown in Figures 2c and 2f for the right and wrong sign combinations. The fitting procedure was checked using simulated events, which were reweighted to mimic $b$-baryon lifetimes between 1.1 ps and 1.6 ps. No significant bias was found.

## 4.4 Lifetime fit result and systematics

The result of the fit was:

$$\tau(\Lambda_c^+\ell) = 1.11^{+0.19}_{-0.17}\ (stat.)\ \text{ps}\ , \tag{4}$$

where the error reflects the statistical contribution only. The fit gave also the flying background lifetimes $\tau_1 = 1.48^{+0.14}_{-0.08}$ ps and $\tau_2 = 0.41^{+0.51}_{-0.17}$ ps with a correlation coefficient with the $b$-baryon lifetime of -0.052 and 0.009, respectively. The fitting procedure was tested using Monte-Carlo samples. No bias was found and the fitted background lifetimes were compatible, within the errors, with the ones obtained on data.

The different contributions to the systematic uncertainty are summarised in Table 2 and detailed as:

- Signal fraction $f_{signal}$ and background parametrisation:
  The signal fraction $f_{signal}$ was varied within its statistical error: the resulting systematic uncertainty was $\pm 0.02$ ps. The background proper time distribution was fitted simultaneously with the signal. Thus, the statistical error quoted above already included the systematic uncertainty related to the background composition and lifetime.
- Resolution functions $P$ and $F$:
  As explained above, the error $\sigma_i$ on the measured decay time $t_i$ was the result of two contributions. The error related to the secondary vertex reconstruction was extensively checked by comparing pull distributions in data and simulation. The simulation prediction concerning the momentum reconstruction was checked in the data using a control sample of 1200 B meson semileptonic decay candidates, reconstructed in the channel $B^0 \to D^+\ell^-\bar{\nu}_\ell X$ followed by $D^+ \to K^-\pi^+\pi^+$. The average momentum measured in real and simulated events agreed at the percent level. The shape of the distribution was used to compare the resolution: possible differences between real and simulated data were found to be smaller than 10%. This was taken into account in the fit by multiplying the error $(\sigma(p)/p)$ in the $\sigma_i$ computation by a scaling factor $1.0 \pm 0.1$.
  The coefficients used in the function $F(t_i, \sigma_i)$, which was used to parametrise the non-flying background, were fitted using the simulation: they were also changed by their uncertainties.
  The resulting systematic uncertainty was $\pm 0.04$ ps.
- $b$-baryon properties:
  The systematic uncertainties related to the $b$-baryon properties were studied by reweighting events and using special simulated samples.
  The uncertainty from the average $b$-baryon energy resulting from $b$-quark fragmentation and from the lepton spectrum from the semileptonic decay modelling was $\pm 0.01$ ps. As mentioned in section 4.2, the flight distance measured in the $\Lambda^0\ell^-\ell^+$

Table 2: Contributions to the systematic uncertainty on the average $b$-baryon lifetime measured using $\Lambda_c^+\ell$ correlations.

| Error source | Values and $\sigma$ used | Syst. error (ps) |
|---|---|---|
| Signal fraction | $0.56 \pm 0.06$ | $\pm 0.02$ |
| Resolution function | see text | $\pm 0.04$ |
| Fragmentation and lepton spectrum | see text | $\pm 0.01$ |
| $\Lambda^0\ell\ell$ flight scaling | $0.90 \pm 0.03$ | $\pm 0.01$ |
| $Br(\Lambda_b^0 \to \Lambda_c^+(\mathrm{n}\pi)\ell^-\bar{\nu}_\ell)/Br(\Lambda_b^0 \to \Lambda_c^+\ell^-\bar{\nu}_\ell)$ | $0.15 \pm 0.15$ | $\pm 0.02$ |
| Total systematic error | – | $\pm 0.05$ |

sample was slightly rescaled. The scaling factor was changed within its errors, and the corresponding systematic uncertainty was $\pm 0.01$ ps. No specific correction was required for the other decay channels.
The dominant uncertainty concerning the $b$-baryon decay modelling is the fraction of non-resonant decays. For such events, a fraction of the $b$-baryon momentum was carried by the additional pions. This was studied, using a special sample of $\Lambda_b^0 \to \Lambda_c^+(\mathrm{n}\pi)\ell^-\bar{\nu}_\ell$ decays. The fraction of such decays was set to 15% and was varied by $\pm 15\%$: the fitted lifetime was changed by $\pm 0.02$ ps.

Summing the systematic uncertainties in quadrature gave an overall systematic uncertainty of $\pm 0.05$ ps. The final result from this analysis was thus:

$$\tau(\Lambda_c^+\ell) = 1.11^{+0.19}_{-0.18}\ (stat.) \pm 0.05\ (syst.)\ \mathrm{ps}\ . \tag{5}$$

# 5 Lifetime measurements using inclusive secondary vertices

Complementary samples containing $b$-baryon decays of the type $\Lambda_b^0 \to \Lambda_c^+\ell^-\bar{\nu}_\ell$ were obtained by searching for inclusive secondary vertices.

## 5.1 Secondary vertex reconstruction and selection

The secondary decay search was originally developed for the study of B mesons [15]. The identified lepton had to have a momentum larger than 3 GeV/$c$. The algorithm tried first to recognize $\Lambda_c^+$ decay products among the other charged particles which belonged to the same jet as the lepton, by clustering them with the LUCLUS algorithm [13] and adding those with the largest pseudo-rapidities (relative to the cluster direction) until the total invariant mass exceeded 2.5 GeV/$c$. The $\Lambda_c^+$ vertex was reconstructed and the procedure was repeated, but using the $\Lambda_c^+$ direction and both charged and neutral particles (including reconstructed $\mathrm{V}^0$'s). The average number of particles selected was 5.3, out of which 2.0 were neutrals. The $\Lambda_c^+$ direction was used, together with the lepton, to fit the $b$-baryon decay vertex. The $b$-baryon momentum was measured using the residual energy method mentioned in section 2.3. The average momentum resolution could be described as the sum of two Gaussian functions of widths 6.3% (for 45% of the events) and 16% (for the rest). The difference between the reconstructed and generated lifetimes

could be described as the sum of two Gaussian functions of widths 0.16 ps (for 68% of the decays) and 0.70 ps (for the rest). In order to enrich the sample in beauty events, the $b$-tagging selection defined in section 2.4 was used and the lepton was required to have a transverse momentum, with respect to the $\Lambda_c^+$ direction, larger than 1.2 GeV/$c$.

The $b$-baryon candidates were selected and grouped in two samples. Events where a reconstructed $\Lambda^0$ was found among the tracks attached to the secondary vertex were grouped into the "$\Lambda^0$-lepton" sample. Events where no reconstructed $\Lambda^0$ but an identified proton was attached to the secondary vertex were grouped into the "proton-lepton" sample.

The number of events common to the semi-exclusive and inclusive samples was found to be very small. This was due to the fact that the inclusive analysis was sensitive to all $\Lambda_c^+$ decays, whereas the kinematical and identification cuts applied to the lepton and proton were softer in the semi-exclusive analyses. Events entering the semi-exclusive sample were removed from the inclusive samples. Therefore, by construction, there was no overlap between the semi-exclusive, proton-lepton and $\Lambda^0$-lepton samples.

## 5.2 Lifetime measurement using the proton-lepton sample

The charged particle with the highest momentum among the $\Lambda_b^0$ decay products, excluding the identified lepton, was required to have a momentum higher than 3 GeV/$c$, and a charge opposite to that of the lepton. It had to be identified as a proton by the RICH detector, and be incompatible with the kaon hypothesis. If the $dE/dx$ measurement was available, it had to be compatible with the proton hypothesis.

### 5.2.1 Composition of the proton-lepton sample

Reconstructed vertices in the $b$-baryon sample could be divided into four classes:

- The signal, where both the identified lepton and the proton originated from a $b$-baryon decay.
- Well reconstructed B meson decays, in which both tracks were originating from the secondary vertex. In the simulation, the number of true protons in this sample was very small. These decays were selected because the leading pion or kaon was misidentified as a proton by the RICH. This class of vertices was referred to as "$B$ mesons".
- Badly reconstructed B decays, in which a particle produced at the primary vertex, in particular a genuine proton, was attached to the secondary vertex and had a momentum higher than all other secondary particles. This class of vertices was referred to as "primary".
- Vertices reconstructed in events originating from light or charm quarks. This class of vertices was referred to as "light".

The simulation predicted a signal purity $f_{signal}$ close to 50%. However, as stressed in section 3, this number depended on the $b$-baryon production fraction and decay branching ratios, which are poorly known. Events with the "wrong sign" combination could not be used to measure the background level, because of the background due to B mesons: high momentum kaons are produced preferentially in the "wrong sign" combination, and the proton/kaon and proton/pion rejection factors obtained with the RICH are not identical. Therefore, the resulting background was not symmetric. However, the sample composition was measured on data, in the following ways.

The measurement of the fraction $f_{light}$ relied on the $b$-tagging probability described in section 2.4 . The cut usually set to enrich the sample was reversed, in order to select events which contained no beauty. The resulting sample was then dominated by "light" vertices, in particular for negative or small proper times. The shape of the proper time distribution was parametrised using the simulation and the only free parameter was the amount of "light vertices". The fit result was unfolded from the $b$-tagging cuts efficiencies and purities, and the fraction $f_{light} = (13 \pm 1)\%$ was determined, in agreement with the simulation.

The fraction $f_{primary}$ was fitted using the reconstructed B momentum distribution. For "signal" and "$B$ meson" vertices, the shape of this distribution reproduced the $b$-quark fragmentation function. This was not the case for "primary" vertices, where particles from the fragmentation were attached to the secondary vertex by mistake: the reconstructed B momentum distribution was approximately flat. This feature was used to fit the amount of such vertices in the total sample: $f_{primary} = (19 \pm 5)\%$ was found, again in agreement with the simulation.

In order to measure the fraction $f_{meson}$ of "$B$ mesons", only the RICH proton selection was applied to the leading particle. Figures 3a-d show, for each class of vertices, the distributions of the difference, $\xi$, between the measured $dE/dx$ value and the one expected for true protons, divided by its error. For "signal" vertices, the proton candidate was a true proton, and the distribution was centered on zero. The leading particles for "$B$ meson" vertices were kaons and pions misidentified by the RICH: kaons were largely suppressed by the required charge correlation, opposite to that of the lepton, and the shape of the distribution was dominated by the pion contribution, which peaked around 2.7. The distribution measured using the total sample was fitted to determine the amount of "$B$ mesons". The fit result was $f_{meson} = (32 \pm 3)\%$ on data. The main systematic uncertainty on this result came from the relative number of kaons and pions contributing to "$B$ meson" vertices. It was measured on data by using similar $dE/dx$ fits, after kaon and pion RICH identification cuts. All resulting systematic uncertainties on $f_{meson}$ were small compared to the statistical error. Then, particles which had a measured $\xi$ larger than 2 were rejected. The final fraction of "$B$ mesons" in the proton-lepton sample was then $f_{meson} = (21 \pm 2)\%$, whereas the simulation predicted 18%.

The fraction $f_{signal}$ of "signal" vertices in the sample was thus measured to be $(47 \pm 5)\%$.

### 5.2.2 Likelihood function for the lifetime fit

The probability $P_s$ to measure a decay time $t_i$ for "signal" vertices was taken to be proportional to:

$$P_s(t_i, \tau) \propto \int_{t=0}^{\infty} A(t) e^{-t/\tau} R(t, t_i) dt \ , \tag{6}$$

where $\tau$ is the $b$-baryon lifetime and $t$ the true decay time; $A(t)$ is the acceptance function (the efficiency to reconstruct the secondary vertex) and $R(t, t_i)$ the resolution function of the proper time measurement. To have a detailed description of the time resolution function $R(t, t_i)$, the distribution of the difference $(t_i - t)$ was parametrised as a function of the true proper time $t$ (using a combination of Gaussian distributions). To obtain the acceptance function $A(t)$, the true time distribution of the simulated events passing the selection cuts was compared with the initial exponential law: the efficiency decreased by at most 10% for small flight distances.

The log-likelihood function was built as the sum of terms, corresponding to the classes of events defined above:

$$\ln L = \Sigma_i \ln f(t_i, \tau) \tag{7}$$

with

$$f(t_i, \tau) = f_{signal} \cdot P_s(t_i, \tau) + f_{meson} \cdot P_m(t_i, \tau_B) + f_{primary} \cdot F_p(t_i) + f_{light} \cdot F_l(t_i) \ , \tag{8}$$

where the fractions $f_{signal}, f_{light}, f_{primary}$ and $f_{meson}$ were fixed to the measured values.

The probability $P_m$ to measure a decay time $t_i$ for "$B$ meson" vertices was studied and parametrised in the same way as the function $P_s$ for "signal" vertices. As explained below, this allowed the "$B$ meson" background lifetime $\tau_B$ to be measured from the data.

The functions $F_l$ and $F_p$ described the time distribution of "light" and "primary" vertices. The time distribution of "light" vertices, which did not contain any B hadron, was parametrised as a sum of Breit-Wigner functions, peaked around zero. For the "primary" vertices, the inclusion of a high momentum particle from fragmentation introduced a shift towards the primary vertex and spoiled the correlation between the measured and the real flight distance. The simulation showed that the resulting time distribution was not sensitive to a change of the B lifetime. The shape was thus parametrised using the simulation, as a sum of Breit-Wigner functions. The simulation was used to check that the procedure did not introduce any bias.

### 5.2.3 Lifetime fit result and systematics

The proton-lepton sample consisted of 499 events, with a purity of 47%. The proper time distributions of the selected samples in real and simulated data are shown in Figure 4. The result of the fit for the value of the $b$-baryon lifetime was:

$$\tau(\mathrm{p}\ell) = 1.19 \pm 0.14 \ (stat.) \ \mathrm{ps} \ . \tag{9}$$

The contributions to the systematic uncertainty are listed in Table 3:

- Signal fraction:
  The fractions of "light", "$B$ meson" and "primary" backgrounds measured on data were changed by $\pm 1\sigma$ to estimate the effect on the likelihood fit result. For the "light" and "primary" vertices, an increase of the background fraction increased the measured lifetime by 0.02 ps and 0.05 ps respectively, whereas an increase of the "$B$ meson" fraction reduced the measured lifetime by 0.03 ps. The three uncertainties were added in quadrature.
- Background lifetime:
  The dominant systematic error related to lifetimes was found to be due to the "$B$ meson" background. The "$B$ meson" background lifetime was fixed to the value measured on data in the following way. A control sample, highly enriched in B mesons, was selected by replacing the proton selection by a pion selection. A likelihood fit, similar to the one described above, was applied to this sample: the lifetime result obtained on data was $\tau_B = 1.61 \pm 0.03$ ps, in agreement with the present world average [16]. The resulting systematic uncertainty on the $b$-baryon lifetime was found to be $\pm 0.03$ ps. The uncertainty on the shapes of "primary" and light background had negligible effect on the $b$-baryon lifetime result.
- Resolution function:
  The resolution function $R(t, t_i)$ was parametrised using the simulation. In a similar way to that explained in section 4.4, the sample enriched in B mesons was used

| Error source | Values and $\sigma$ used | Syst. error (ps) |
|---|---|---|
| signal fraction | $0.47 \pm 0.05$ | $\pm$ 0.06 |
| background lifetime | $1.61 \pm 0.03$ ps | $\pm$ 0.03 |
| resolution function | see text | $\pm$ 0.02 |
| $\Lambda_b^0$ and $\Lambda_c^+$ decay | see text | $\pm$ 0.01 |
| Total systematic error | - | $\pm$ 0.07 |

Table 3: Contributions to the systematic uncertainty (in ps) for the proton-lepton channel.

to check extensively the Monte-Carlo predictions concerning the flight distance and energy measurement. No significant difference between data and simulation was found. This was also confirmed by the measured "$B$ meson" background lifetime which agreed, within the statistical uncertainty of 0.03 ps, with the present world average value. The parameters used to describe the resolution function $R(t, t_i)$ were fitted using simulated events: they were changed within their errors. The overall systematic uncertainty was found to be $\pm 0.02$ ps.

- $b$-baryon properties:
  In the semi-exclusive analysis, the dominant uncertainty was found to be related to non-resonant $\Lambda_b^0 \to \Lambda_c^+(\mathrm{n}\pi)\ell^-\bar{\nu}_\ell$ decays. The inclusive sample could include, a priori, a wider range of non-resonant decays, not necessarily involving a $\Lambda_c^+$, but the sensitivity was much reduced for two reasons. First, because the lepton transverse momentum spectrum is softer for such decays. With the cut used in this analysis, which is twice harder than the one used for semi-exclusive channels, the selection efficiency was found to be 40% of that obtained for $\Lambda_\mathrm{b}^0 \to \Lambda_c^+\ell^-\bar{\nu}_\ell$ decays. Furthermore, in 30% of the selected non-resonant events, some of the additional pions were attached to the secondary vertex and the $\Lambda_b^0$ momentum estimation was correct. As a consequence, the systematic error related to non-resonant decays was found to be negligible.
  On the other hand, the sample selected in this inclusive analysis was a mixture of events where the proton was produced directly (e.g. via $\Lambda_c^+ \to pK^-\pi^+$ decay), or via a $\Lambda^0$ which was not reconstructed. The presently measured branching fractions [16] were used to estimate that the ratio between the $\Lambda_c^+ \to pX$ and $\Lambda_c^+ \to \Lambda^0 X$ branching fractions could vary between 0.75 and 0.4, whereas it had been set to 0.7 in the simulation. As the resolution of the lifetime measurement was predicted to be slightly different for these two cases, events were reweighted to study this effect in detail. The resulting systematic uncertainty was found to be smaller than 0.01 ps. A similar study was performed to compare the resolution for events in which $\mathrm{K}^0$'s and $\pi^0$'s were produced. All effects were negligible.
  The systematic uncertainty related to the $b$-baryon and $\Lambda_c^+$ decay properties was thus conservatively set to $\pm 0.01$ ps.

As a result of this study, the dominating systematic uncertainties were due to the background level, measured on data and thus independent of Monte-Carlo assumptions. The numbers quoted in Table 3 were added in quadrature, and the lifetime fit result was:

$$\tau(\mathrm{p}\ell) = 1.19 \pm 0.14\ (stat.) \pm 0.07\ (syst.)\ \mathrm{ps}\ . \qquad (10)$$

## 5.3 Lifetime measurement using $\Lambda^0$-lepton correlations

The sample used in this analysis was obtained by demanding a reconstructed $\Lambda^0$ among the particles attached to the secondary vertex. The $\Lambda^0$ selection cuts were summarised in section 2.2.3. The particle with the highest momentum of the $\Lambda^0$ decay products had to be identified as a proton and to have a charge opposite to that of the lepton. The $\Lambda^0$ momentum had to be larger than 2.5 GeV/$c$.

### 5.3.1 Composition of the $\Lambda^0$-lepton sample and likelihood function

The signal and background contributions in the $\Lambda^0$-lepton sample could be grouped into the same four classes as in the proton-lepton channel analysis: "signal","light", "primary" and "$B$ meson" vertices. However, in this sample the simulation predicted that all backgrounds were contributing in the same way in the "right sign" and "wrong sign" $\Lambda^0$-lepton combinations within a precision better than $\pm 10\%$, and had the same proper time distribution in both sign combinations. Therefore,"wrong sign" events were used to parametrise the total background.

262 events were selected in the "right sign" and 172 events in the "wrong sign" combinations, giving a signal purity $f_{signal} = (34 \pm 6)\%$.

The likelihood function used in the lifetime fit was similar to the one used in the proton-lepton channel analysis, but restricted to two terms:

$$\ln L = \Sigma_i \ln f(t_i, \tau) \tag{11}$$

with

$$f(t_i, \tau) = f_{signal} \cdot P_s(t_i, \tau) + (1 - f_{signal}) \cdot F_{opp}(t_i) \; , \tag{12}$$

where the signal distribution $P_s$ was obtained by the convolution of an exponential function with the resolution function $R(t, t_i)$, parametrised as in the proton-lepton analysis described in section 5.2.2. The background distribution was parametrised on data using the "wrong sign" sample.

### 5.3.2 Lifetime fit result and systematics

The proper time distributions of the "right sign" and "wrong sign" samples are shown in Figures 5a,b. For the "right sign" sample, the curves show the result of the likelihood fit. The result is:

$$\tau(\Lambda^0 \ell) = 1.16 \pm 0.20 \; (stat.) \text{ ps} \; . \tag{13}$$

The values of the systematics are summarised in Table 4:

- Background level and lifetime:
  The total number of "wrong sign" events was measured with a statistical precision of $\pm 8\%$: the resulting change in the $b$-baryon lifetime was $\pm$ 0.02 ps. The parametrisation used for the proper time shape, fitted on the "wrong sign" sample, was also varied within its errors. The resulting systematic uncertainty was $\pm 0.08$ ps.
- Resolution function and $b$-baryon properties:
  In a similar way to the other analyses, the description of the resolution function was varied. All effects were found to be smaller than 0.02 ps.

The dominating systematic uncertainties were found to be independent of Monte-Carlo assumptions, and the lifetime fit result was:

$$\tau(\Lambda^0 \ell) = 1.16 \pm 0.20 \; (stat.) \pm 0.08 \; (syst.) \text{ ps} \; . \tag{14}$$

| Error source | Values and $\sigma$ used | Syst. error (ps) |
|---|---|---|
| signal fraction | $0.34 \pm 0.06$ | $\pm$ 0.02 |
| background lifetime | see text | $\pm$ 0.08 |
| resolution function | see text | $\pm$ 0.02 |
| Total systematic error | - | $\pm$ 0.08 |

Table 4: Contributions to the systematic uncertainty (in ps) for the $\Lambda^0$-lepton channels.

# 6 Final result and conclusion

The average lifetime of the $b$-baryon was measured using three different samples, selected by the presence, in the same jet, of a high $p_T$ lepton and a fast $\Lambda_c^+$, proton, or $\Lambda^0$:

$$\begin{aligned} \tau(\Lambda_c^+\ell) &= 1.11^{+0.19}_{-0.18}\ (stat.) \pm 0.05\ (syst.)\ \text{ps} \\ \tau(\text{p}\ell) &= 1.19 \pm 0.14\ (stat.)\ \pm 0.07\ (syst.)\ \text{ps} \\ \tau(\Lambda^0\ell) &= 1.16 \pm 0.20\ (stat.)\ \pm 0.08\ (syst.)\ \text{ps}\ . \end{aligned}$$

Only 15% of the exclusive $\Lambda_c^+\ell^-$ vertices passed the selections used in the inclusive analyses, due to the tight requirement on the lepton transverse momentum and proton identification. These events were removed from the inclusive samples and, therefore, there was no statistical overlap between the three samples.

The systematics related to the parametrisation of the resolution function depended on Monte-Carlo assumptions, regarding both the $b$-baryon properties and the simulation of the detector characteristics. Therefore, they were considered as fully correlated in the three lifetime measurements.

These new measurements replace all previously published DELPHI results, in particular the references [6,7], except for the analysis based on the impact parameter distribution of identified muons, associated with a high momentum $\Lambda^0$ [7], whose result was:

$$\tau(\text{impact}) = 1.10^{+0.19}_{-0.17}\ (stat.) \pm 0.09\ (syst.)\ \text{ps}\ .$$

Due to the different kinematical and $b$-tagging cuts, only 20% of the events used in the $\Lambda^0$-lepton analysis passed the selection cuts of the impact parameter analysis. The systematic uncertainties were uncorrelated, since the dominant one for the impact parameter analysis was the effect of the $\Lambda_b^0$ polarisation, which does not affect the new measurements, based on reconstructed secondary vertices.

Taking into account the correlations, the combination of the four lifetime determinations gave the result:

$$\tau(b-\text{baryon}) = 1.14 \pm 0.08\ (stat.) \pm 0.04\ (syst.)\ \text{ps}\ .$$

This measurement confirms the discrepancy between the measured and expected $b$-baryon lifetime. It should be stressed that these results correspond to lifetime averages of different $b$-baryons, weighted by their production rates in $b$-jets at LEP and their semileptonic branching ratios into the considered channels. However, the expected production rates and selection efficiencies are such that all samples are expected to be dominated by $\Lambda_b^0$ baryons.

## Acknowledgements

We are greatly indebted to our technical collaborators, to the members of the CERN-SL Division for the excellent performance of the LEP collider, and to the funding agencies for their support in building and operating the DELPHI detector.
We acknowledge in particular the support of
Austrian Federal Ministry of Science and Traffics, GZ 616.364/2-III/2a/98,
FNRS–FWO, Belgium,
FINEP, CNPq, CAPES, FUJB and FAPERJ, Brazil,
Czech Ministry of Industry and Trade, GA CR 202/96/0450 and GA AVCR A1010521,
Danish Natural Research Council,
Commission of the European Communities (DG XII),
Direction des Sciences de la Matière, CEA, France,
Bundesministerium für Bildung, Wissenschaft, Forschung und Technologie, Germany,
General Secretariat for Research and Technology, Greece,
National Science Foundation (NWO) and Foundation for Research on Matter (FOM), The Netherlands,
Norwegian Research Council,
State Committee for Scientific Research, Poland, 2P03B06015, 2P03B03311 and SPUB/P03/178/98,
JNICT–Junta Nacional de Investigação Científica e Tecnológica, Portugal,
Vedecka grantova agentura MS SR, Slovakia, Nr. 95/5195/134,
Ministry of Science and Technology of the Republic of Slovenia,
CICYT, Spain, AEN96–1661 and AEN96-1681,
The Swedish Natural Science Research Council,
Particle Physics and Astronomy Research Council, UK,
Department of Energy, USA, DE–FG02–94ER40817.

# References


[1] ALEPH Collaboration, D. Decamp *et al.*, Phys. Lett. **B278** (1992) 209;
OPAL Collaboration, P. D. Acton *et al.*, Phys. Lett. **B281** (1992) 394.
[2] DELPHI Collaboration, P. Abreu *et al.*, Phys. Lett. **B311** (1993) 379.
[3] ALEPH Collaboration, D. Buskulic *et al.*, Phys. Lett. **B297** (1992) 449;
OPAL Collaboration, R. Akers *et al.*, Phys. Lett. **B316** (1993) 435.
[4] I.I. Bigi and N.G. Uraltsev, Phys. Lett. **B280** (1992) 271;
I.I. Bigi, "Lifetimes of Heavy Flavour Hadrons", UND-HEP-95-BIG06, Proc. of 6th Int. Symp. on Heavy Flavour Physics, Pisa, Italy, June 1995, eds. F.Costantini and M. Giorgi, Compositori, Bologna.
[5] ALEPH Collaboration, D. Buskulic *et al.*, Phys. Lett. **B357** (1995) 685;
OPAL Collaboration, R. Akers *et al.*, Phys. Lett. **B353** (1995) 402;
OPAL Collaboration, R. Akers *et al.*, Z. Phys. **C69** (1996) 195;
CDF Collaboration, F. Abe *et al.*, Phys. Rev. Lett. **77** (1996) 1439.
[6] DELPHI Collaboration, P. Abreu *et al.*, Z. Phys. **C68** (1995) 375.
[7] DELPHI Collaboration, P. Abreu *et al.*, Z. Phys. **C71** (1996) 199.
[8] DELPHI Collaboration, P. Aarnio *et al.*, Nucl. Instr. Meth. **A303** (1991) 233.
[9] DELPHI Collaboration, P. Abreu *et al.*, Nucl. Instr. Meth. **A378** (1996) 57.
[10] V. Chabaud *et al.*, Nucl. Instr. Meth. **A368** (1996) 314.
[11] DELPHI Collaboration, P. Abreu *et al.*, Nucl. Phys. **B418** (1994) 403.
[12] E.G. Anassontzis *et al.*, Nucl. Instr. Meth. **A323** (1992) 351.
[13] T. Sjöstrand, Comp. Phys. Comm. **82** (1994) 74.
[14] DELPHI Collaboration, P. Abreu *et al.*, Z. Phys. **C57** (1993) 181.
[15] DELPHI Collaboration, P. Abreu *et al.*, Z. Phys. **C74** (1997) 19.
[16] Particle Data Group, "Review of Particle Properties", Euro. Phys. J. **C3** (1998) 1.
[17] G.V. Borissov and C. Mariotti, Nucl. Instr. and Meth. **A372** (1996) 181;
Contribution to ICHEP'98 number 123, DELPHI 98-123, CONF 184.
[18] DELPHI Collaboration, P. Abreu *et al.*, Z. Phys. **C68** (1995) 541.
[19] V. Gibson, Proc. of XXVII International Conference on High Energy Physics, eds. P.J. Bussey and I.G. Knowles, IOP (1994), 507.
[20] N. Isgur and M.B. Wise, Phys. Lett. **B232** (1989) 113;
N. Isgur and M.B. Wise, Phys. Lett. **B237** (1990) 527.
[21] F. Abe *et al.*, Phys. Rev. **D55** (1997) 1142.
[22] CLEO Collaboration, G. Crawford *et al.*, Phys. Rev. **D45** (1992) 752.

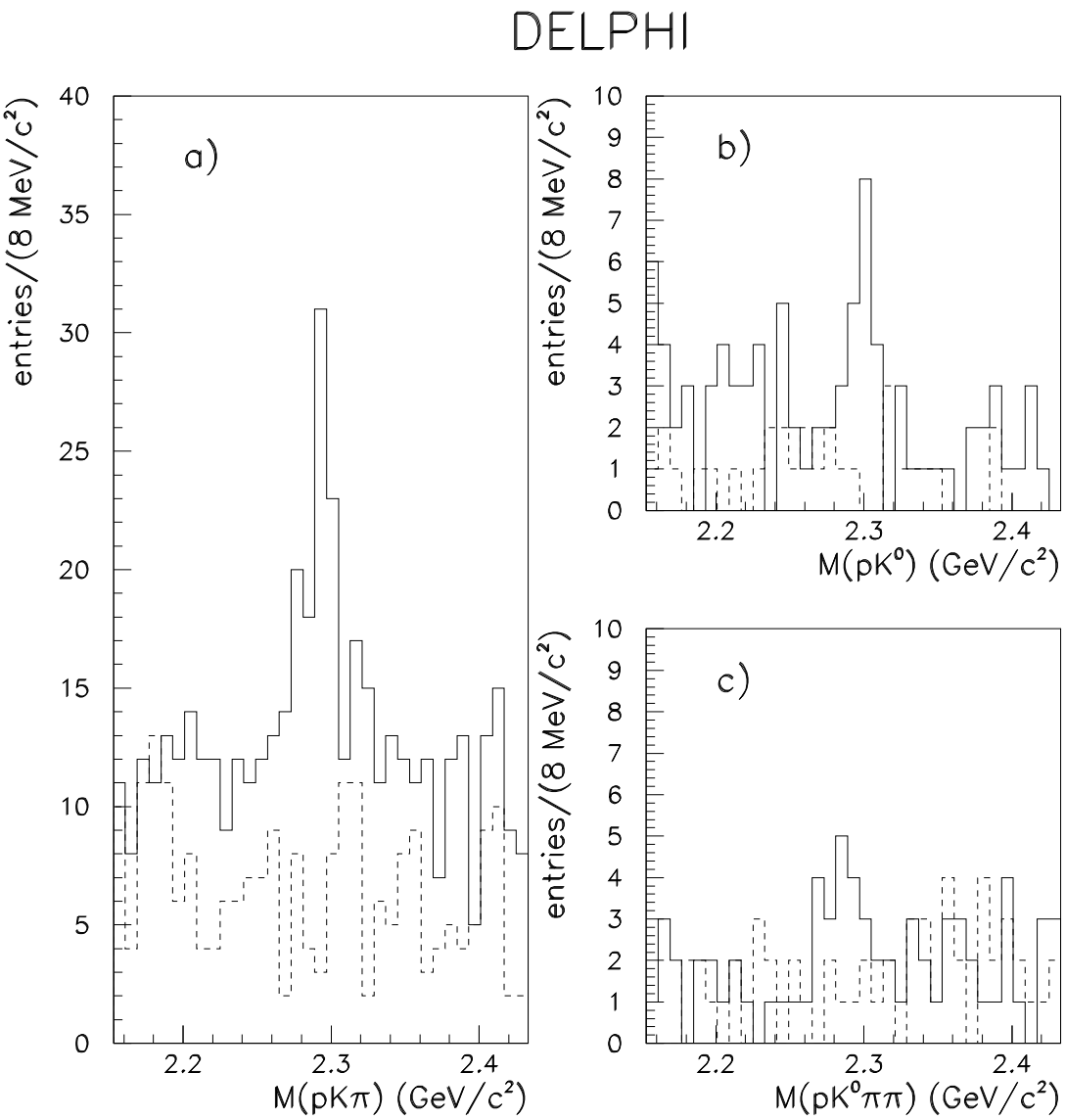


Figure 1: Reconstructed invariant mass distributions for $\Lambda_c^+$ vertex candidates correlated with a high $p_T$ lepton: a) $pK\pi$, b) $pK^0$ and c) $pK^0\pi\pi$ channels. The full line (dashed line) histograms are the "right sign" $\Lambda_c^+\ell^-$ ("wrong sign" $\Lambda_c^+\ell^+$) combinations.

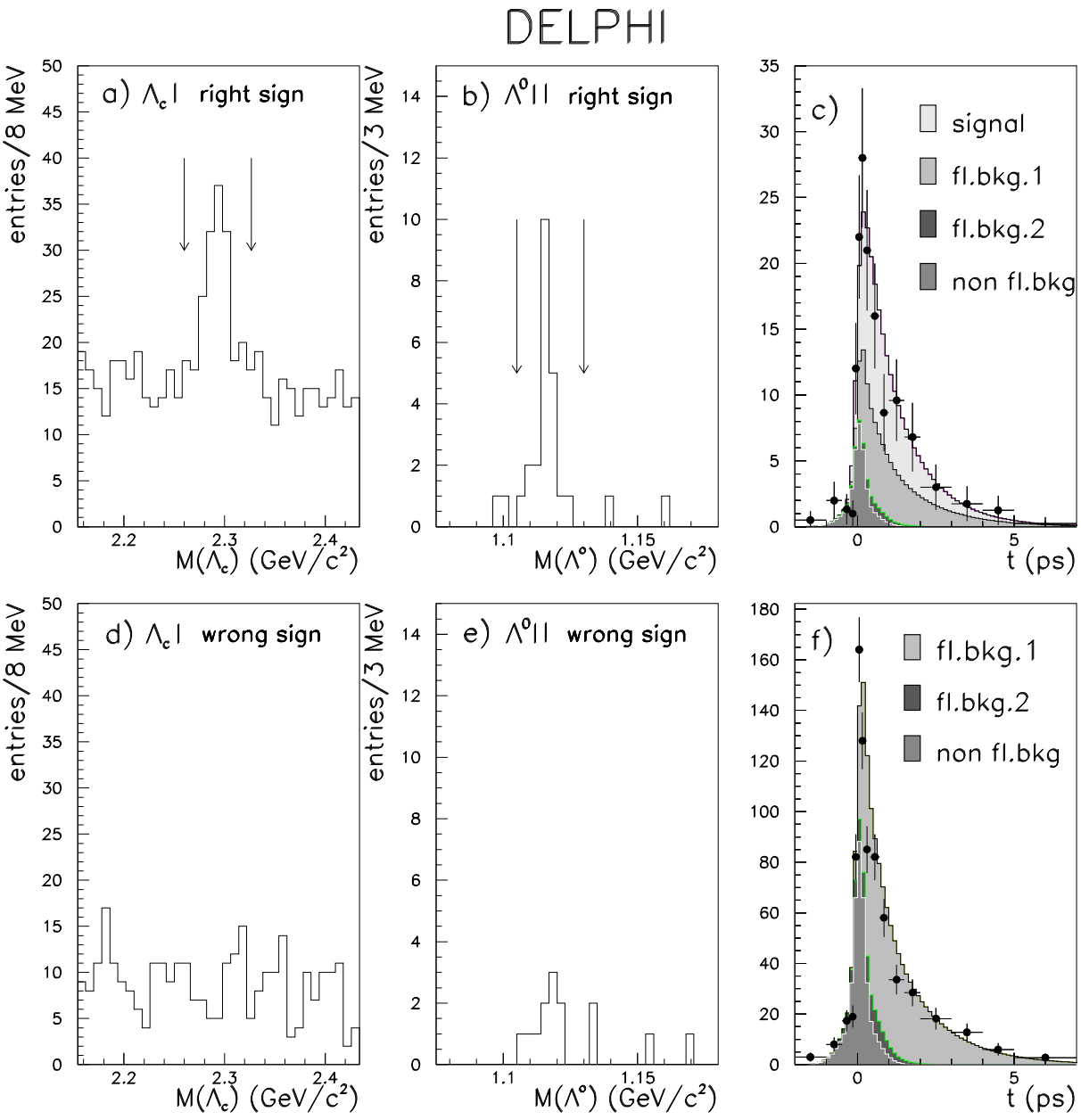


Figure 2: Invariant mass distribution for a) $\Lambda_c^+$ candidates and b) $\Lambda^0$ candidates in right sign combinations; the arrows show the invariant mass regions defining the "signal samples"; c) proper time distribution for the corresponding $b$-baryon candidates of the two signal samples combined; d-f) same for wrong sign combinations (see text for definition). The histograms superimposed to the data points in c) and f) show the different components resulting from the likelihood fit described in the text.

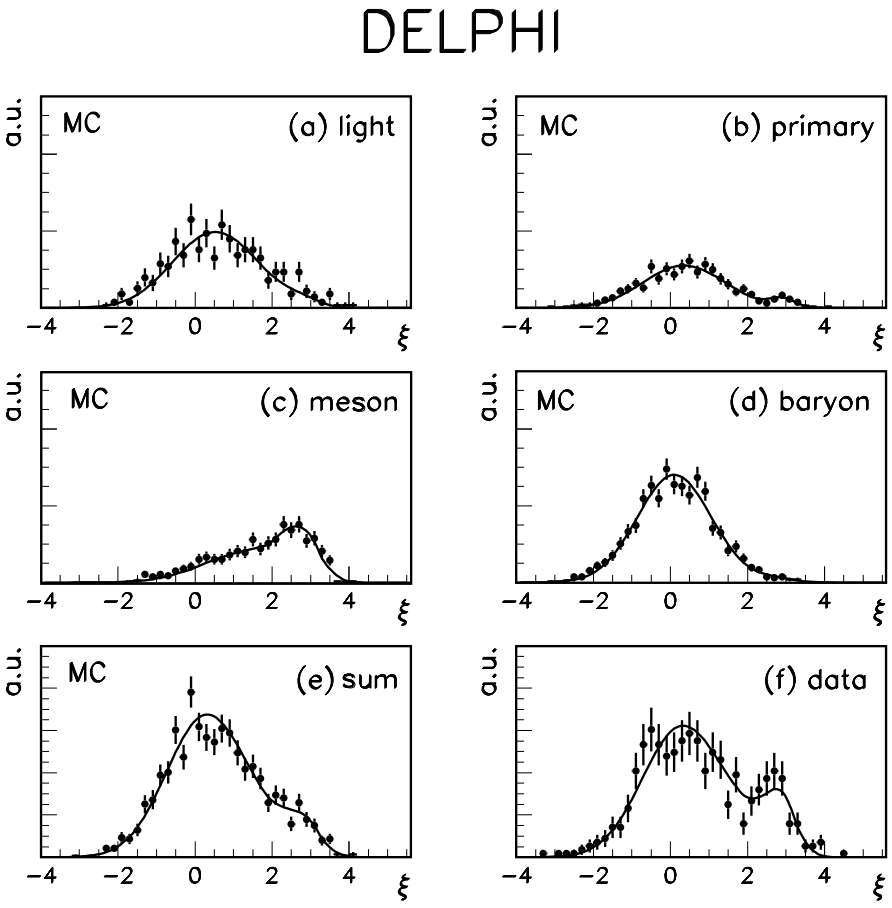


Figure 3: Distributions of the difference, $\xi$, between the measured $dE/dx$ value and the one expected for a proton, normalized to the error, for the proton candidate identified by the RICH detector. The fitted function is superimposed to the distribution predicted by the simulation for each vertex class (a to d). For clarity, the distributions have been normalised to their relative contributions in the Monte-Carlo sample. The total distribution and the fit result are shown for the simulation (e) and the data (f). The vertical scale is in arbitrary units (a.u.).

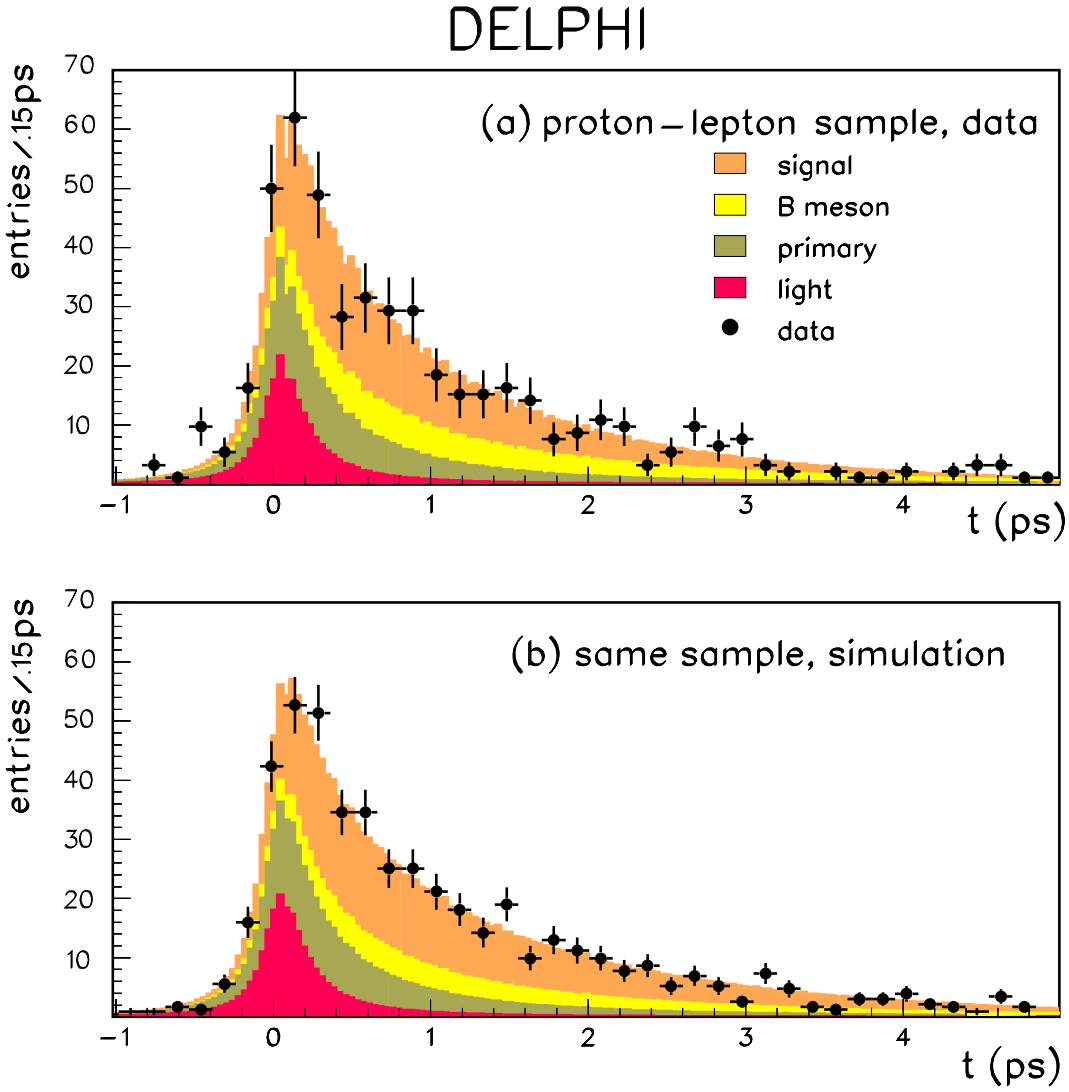


Figure 4: Proper time distributions of the proton-lepton sample (a) on data and (b) on simulation. The sample distributions (dots) are superimposed on the result of the fit. The contribution of each class of vertices is also shown.

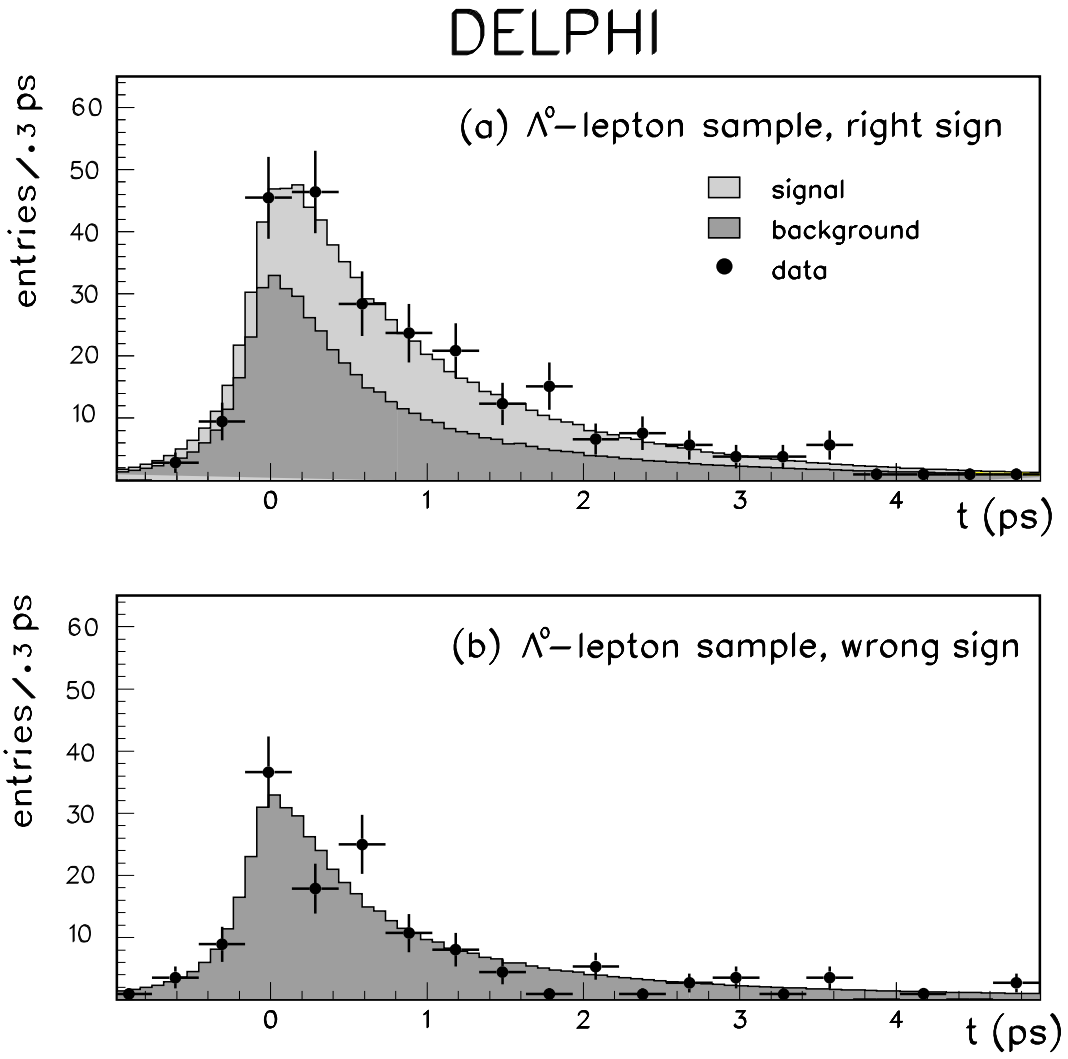


Figure 5: Proper time distributions for the $\Lambda^0$-lepton samples with (a) the "right sign" and (b) the "wrong sign" correlations. The sample distributions (dots) are superimposed on the result of the fit.